Chapter 5

Meshing Skin Surfaces

This chapter appeared as [75] and is accepted to Computational Geometry, Theory and Applications as [76].

5.1 Introduction

We present an algorithm for meshing skin surfaces with guaranteed topology. The algorithm presented in this chapter constructs a mesh isotopic to the skin surface in two steps: it constructs a coarse, isotopic mesh which is subsequently improved by refinement algorithms. The complexity of the coarse mesh is quadratic in the number of input balls, and is independent of the shrink factor. This is worst case optimal. For the second step a broad range of refinement algorithms can be used. Existing algorithms may have to be adapted slightly to ensure the isotopy. We show how this is done for the refinement algorithms of Chew [34] and Kobbelt [69]. The $\sqrt{3}$-subdivision algorithm by Kobbelt is very fast, and refines the size of the triangles. However, it does not improve the quality of the mesh elements in terms of angle size. Chew's algorithm improves the quality of the mesh in terms of the angles and the size of the triangles in terms of a measure like the circumradius or the length of the longest edge. The quality mesh is suitable for numerical computations. Our version of these algorithms preserve the isotopy property. Methods like the one presented in [44] are also well suited for mesh enhancements.

Related work Most existing algorithms for meshing implicit surfaces do not guarantee topological equivalence of the surface and the mesh constructed. The marching cubes algorithm [82] subdivides a region into cubes and triangulates the surface within these cubes based on whether the vertices of the cube lie inside or outside the cube. A variant of this algorithm that follows the surface is presented in [17].

The marching triangulation method [62] extends a small initial mesh by walking over the implicit surface, starting from a seed point. Our paper [73] presents a marching triangulation method for meshing skin surfaces by carefully choosing the step size during the walk over the mesh. However, as the shrink factor goes to one or to zero, the size of the mesh goes to infinity.

Several algorithms [27, 29, 30, 51] have been proposed to construct a topologically correct mesh approximating a skin surface in the special case of a shrink factor 1/2. It is likely that these algorithms can be generalized to work for arbitrary shrink factors, but this will result in a denser mesh in order to guarantee the topology and will therefore yield slower running times.

The algorithms in [27, 51] construct a dense point sample on the skin surface and use a three-dimensional Delaunay triangulation to extract the mesh from these points. These algorithms are rather slow compared to the other algorithms [29, 30].

Another approach is presented in [29]. The algorithm is competitive in terms of running times. We could not verify the claim that the mesh produced by the algorithm in this paper is homeomorphic to the skin surface. In fact, in [30] the authors say the following. "This method improved the efficiency dramatically (with respect to [27]) but resulted in robustness problem of the implementation ...The accumulation of numerical errors in the approximation of Morse-Smale complex led to inconsistent critical points after eliminating noisy critical points inaccurately."

The recent algorithm in [30] uses the theoretical results from [27] combined with ideas of the advancing front from [29]. The mesh is constructed by advancing the mesh over the skin surface while maintaining the restricted Delaunay triangulation.

Another method for visualizing molecules uses Molecular Surfaces [38]. Visualization algorithms for this type of surface are presented in [14, 15]. The algorithms presented in [21, 85] are the first general methods guaranteeing topological equivalence of the implicit surface and the mesh.

Contribution The approach to meshing skin surfaces described in this chapter is new. The main contribution compared to [27] is that our approach works for any shrink factor. We also establish isotopy, which is stronger than topological equivalence. Our algorithm is more flexible in the sense that we generate a coarse mesh that is isotopic to the skin surface that can subsequently be refined by various algorithms, as shown in Section 5.3.4, whereas the algorithm in [27] immediately constructs a homeomorphic quality mesh. Further, our algorithm is much faster. It constructs a mesh in minutes where the algorithm presented in [27] takes hours.

On the theoretical side, we analyze the structure of the mixed complex and decompose the mixed cells into tetrahedra. Within a tetrahedron the intersection with the skin surface is either empty or a topological disk. It is fairly easy to extract the isotopic mesh from this tetrahedral complex by a marching tetrahedra algorithm.

Outline In Section 5.2 we extend the theory of skin surfaces as presented in [48]. We start by introducing a hierarchical combinatorial structure on the mixed complex. With each face of this complex we associate an anchor point, which plays a crucial role in the meshing algorithm. Section 5.3 describes the construction of the coarse mesh and establishes the isotopy between this mesh and the skin surface. In Section 5.3.4, we describe two methods to improve the coarse mesh via (i) subdivision of the triangles and (ii) improvement of the quality of the triangles with regard to the size of the minimal angle. Finally, we describe our implementation and give experimental results in Section 5.4 and 5.5.

5.2 Definitions

This section first briefly reviews skin surfaces and then introduces some new concepts specific to the meshing algorithm. For a more thorough introduction to skin surfaces, we refer to Section 2.7 and to [48] where they were originally introduced.

5.2.1 Skin surfaces

A skin surface is defined in terms of a finite set of weighted points $\mathcal{P}$ and a shrink factor s, with $0 \leq s \leq 1$. A weighted point $\hat{p} = (p, P) \in \mathbb{R}^d \times \mathbb{R}$ corresponds to a ball with center p and radius $\sqrt{P}$. A pseudo-distance between two weighted points is given by:

$$\pi(\hat{p}, \hat{q}) = \|p - q\|^2 - P - Q,$$

where $\hat{p} = (p, P)$, $\hat{q} = (q, Q)$ and $\|\cdot\|$ denotes the Euclidean distance. The pseudo-distance $\pi(\hat{p}, x)$ of a weighted point $\hat{p}$ to an (unweighted) point x is the pseudo-distance of $\hat{p}$ to the weighted point centered at x with zero weight. Two weighted points with zero distance are called *orthogonal*. An *orthosphere* of a set of weighted points $\mathcal{P}$ is, by definition, a sphere orthogonal to each of the weighted points in $\mathcal{P}$.

The space of weighted points inherits a vector space structure from $\mathbb{R}^{d+1}$ via the bijective map $\Pi : \mathbb{R}^d \times \mathbb{R} \to \mathbb{R}^{d+1}$, defined by $\Pi(\hat{p}) = (x_1, \ldots, x_d, \|p\|^2 - P)$, with $p = (x_1, \ldots, x_d)$. Addition of two weighted points and the multiplication of a weighted point by a scalar are defined in the vector space structure inherited under Π. For further reading on the space of circles and spheres we refer to [84, 41].

Starting from a weighted point $\hat{p} = (p, P)$, the shrunk weighted point $\hat{p}^s$ is defined as $\hat{p}^s = (p, s \cdot P)$. The set $\mathcal{P}^s$ is the set obtained by shrinking every weighted point of $\mathcal{P}$ by a factor s.

The skin surface $\mathrm{skn}^s(\mathcal{P})$ and its body $\mathrm{bdy}^s(\mathcal{P})$ associated with a set of weighted points $\mathcal{P}$, are defined by

$$\mathrm{bdy}^s(\mathcal{P}) = \cup(\mathrm{conv}\,\mathcal{P})^s$$
$$\mathrm{skn}^s(\mathcal{P}) = \partial\ \mathrm{bdy}^s(\mathcal{P}).$$

Here $\mathrm{conv}(\mathcal{P}) \subset \mathbb{R}^d \times \mathbb{R}$ is the convex hull – with respect to the vector space structure inherited under Π – of a set of weighted points $\mathcal{P}$, whereas ∂ denotes the boundary – in $\mathbb{R}^d$ – of the union of the corresponding set of set of balls. For a skin curve in 2D associated with two weighted points: see Figure 5.1.

5.2.2 Delaunay triangulation

The Delaunay triangulation and Voronoi diagram are used to decompose the skin surface into patches of spheres and hyperboloids. We briefly give the definition of these structures and mention some properties.

The (weighted) Voronoi diagram (or: the power diagram) $\mathrm{Vor}(\mathcal{P})$ of a set of weighted points $\mathcal{P}$ is the subdivision of $\mathbb{R}^d$ into cells $\nu_{\mathcal{X}}$ that have smaller power

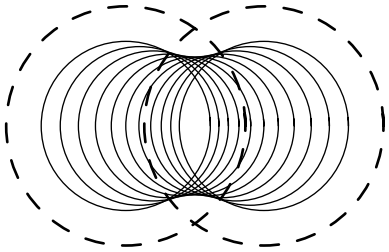

Figure 5.1: The skin curve of two weighted points (the two dashed circles). The smaller circles form a subset of the shrunk convex hull of the input points. Its boundary forms the skin curve.

distance to the weighted points in $\mathcal{X} \subseteq \mathcal{P}$ than to any other weighted point in $\mathcal{P}$:

$$\nu_{\mathcal{X}} = \bigcap_{\hat{p} \in \mathcal{X}, \hat{p}' \in \mathcal{P}} \{x \in \mathbb{R}^d | \pi(\hat{p}, x) \leq \pi(\hat{p}', x)\}.$$

Observation 40. *Let $y_{\hat{p},\hat{p}'}$ be a point with the same power distance to $\hat{p}$ and $\hat{p}'$, then $\nu_{\mathcal{X}} = \bigcap_{\hat{p} \in \mathcal{X}, \hat{p}' \in \mathcal{P}} \{x \in \mathbb{R}^d | \langle x - y_{\hat{p},\hat{p}'}, p' - p \rangle \leq 0\}$*

Proof. We have

$$\begin{aligned} & \pi(\hat{p}, x) \leq \pi(\hat{p}', x) \\ \equiv \quad & \|p - x\|^2 - P \leq \|p' - x\|^2 - P' \\ \equiv \quad & 2\langle x, p' - p \rangle \leq P - P' + \|p'\|^2 - \|p\|^2 \\ \equiv \quad & 2\langle x, p' - p \rangle \leq 2\langle y_{\hat{p},\hat{p}'}, p' - p \rangle \\ \equiv \quad & \langle x - y_{\hat{p},\hat{p}'}, p' - p \rangle \leq 0. \end{aligned}$$

Hence, the proof follows from the definition of a Voronoi cell. □

The dual of the Voronoi diagram is the Delaunay triangulation (or: regular triangulation) $\mathrm{Del}(\mathcal{P})$. We denote a Delaunay simplex of a set $\mathcal{X} \subseteq \mathcal{P}$, with $\nu_{\mathcal{X}} \neq \emptyset$, by $\delta_{\mathcal{X}}$. Recall that $\delta_{\mathcal{X}} = \mathrm{conv}(\{p | \hat{p} \in \mathcal{X}\})$. If $\mathcal{X} \subsetneq \mathcal{X}'$ and $\nu_{\mathcal{X}'} \neq \emptyset$, then $\nu_{\mathcal{X}'}$ is a proper face of $\nu_{\mathcal{X}}$ and $\delta_{\mathcal{X}}$ is a proper face of $\delta_{\mathcal{X}'}$.

The affine hulls of a Delaunay simplex $\delta_{\mathcal{X}}$ and its dual Voronoi cell $\nu_{\mathcal{X}}$ are complementary and orthogonal. Hence, the affine hulls of $\delta_{\mathcal{X}}$ and $\nu_{\mathcal{X}}$ always intersect in a single point, the focus $f(\mathcal{X})$ of $\mathcal{X}$.

General position In the remainder of this chapter we assume general position, by which we mean that no $d+2$ weighted points are equidistant to a point in $\mathbb{R}^d$ and no $k+2$ centers of weighted points lie on a common k-flat for $k = 0, \ldots, d-1$. Several methods like [50] exist to symbolically perturb a data set and ensure these conditions. Note that, under this genericity condition, an orthosphere of a set $\mathcal{X}$ only exists if $|\mathcal{X}| \leq d+1$.

Consider a Delaunay cell $\delta_{\mathcal{X}'}$ and one of its faces $\delta_{\mathcal{X}}$, with $\mathcal{X} \subsetneq \mathcal{X}'$. Their duals are respectively a face of a Voronoi cell and the Voronoi cell itself. There is

a halfspace through $\delta_{\mathcal{X}}$ containing $\delta_{\mathcal{X}'}$ and a halfspace through $\nu_{\mathcal{X}'}$ containing $\nu_{\mathcal{X}}$ such that their normals point in opposite directions.

Lemma 41. *Let $\delta_{\mathcal{X}}, \delta_{\mathcal{X}'} \in \mathrm{Del}(\mathcal{P})$, such that $\delta_{\mathcal{X}}$ is a proper face of $\delta_{\mathcal{X}'}$ and let $u = x'_\delta - x_\delta$ with $x_\delta \in \delta_{\mathcal{X}}$, $x'_\delta \in \mathrm{int}(\delta_{\mathcal{X}'})$. Then*

1. $\langle u, x_\nu - x'_\nu \rangle = 0$, *for* $x_\nu, x'_\nu \in \nu_{\mathcal{X}'}$.
2. $\langle u, x_\nu - x'_\nu \rangle < 0$, *for* $x_\nu \in \nu_{\mathcal{X}} \setminus \nu_{\mathcal{X}'}$, $x'_\nu \in \nu_{\mathcal{X}'}$

Proof. Claim (1) follows directly from the orthogonality of $\delta_{\mathcal{X}'}$ and $\nu_{\mathcal{X}'}$, cf. Observation 1. Hence, claim (2) is independent of the choice of x'_ν.

For the proof of claim (2), let $m = |\mathcal{X}|$, $n = |\mathcal{X}'|$ and $\mathcal{X}' = \{\hat{p}_1, \ldots, \hat{p}_n\}$, such that $\hat{p}_i \in \mathcal{X}$, for $i \leq m$. Write x_δ and x'_δ in barycentric coordinates: $x_\delta = \sum \gamma_i \cdot p_i$, $x'_\delta = \sum \gamma'_i \cdot p_i$ with $\sum \gamma_i = \sum \gamma'_i = 1$, $\gamma_i, \gamma'_i \geq 0$. Since $x_\delta \in \delta_{\mathcal{X}}$, $\gamma_i = 0$ for $i \geq m+1$, and $\gamma'_i > 0$ since $x'_\delta \in \mathrm{int}(\delta_{\mathcal{X}'})$. Rewrite u as:

$$\begin{aligned} u &= x'_\delta - x_\delta \\ &= \sum_{i=1}^{m} (\gamma'_i - \gamma_i) p_i + \sum_{i=m+1}^{n} \gamma'_i p_i \\ &= \sum_{i=1}^{m} (\gamma'_i - \gamma_i)(p_i - p_1) + \sum_{i=m+1}^{n} \gamma'_i (p_i - p_1) \end{aligned}$$

Expanding $\langle u, x_\nu - x'_\nu \rangle$ yields:

$$\begin{aligned} \langle u, x_\nu - x'_\nu \rangle &= \sum_{i=1}^{m} (\gamma'_i - \gamma_i) \langle p_i - p_1, x_\nu - x'_\nu \rangle \\ &\quad + \sum_{i=m+1}^{n} \gamma'_i \langle p_i - p_1, x_\nu - x'_\nu \rangle \end{aligned}$$

From Observation 40, with $y_{\hat{p}_i, \hat{p}_1} = x'_\nu$, it follows that $\langle p_i - p_1, x_\nu - x'_\nu \rangle$ is not positive. Moreover, the inner product is zero if and only if $\hat{p}_i \in \mathcal{X}$. Hence, the elements of the first sum are zero and the elements of the second sum are negative, so $\langle u, x_\nu - x'_\nu \rangle < 0$. Note that for $\hat{p}_1$ we can substitute any weighted point in $\mathcal{X}$. □

Although the meshing algorithm generalizes to any dimension, the main application is in $\mathbb{R}^3$. Therefore we present the algorithm in three space.

5.2.3 The mixed complex

We already described the mixed complex in Section 2.7.4. In this section we give a more thorough presentation of the mixed complex and derive its polyhedral structure.

The mixed complex $\mathrm{Mix}^s(\mathcal{P})$, associated with a scalar $s \in [0, 1]$, is an intermediate complex between the Delaunay triangulation and the Voronoi diagram. Each mixed cell in the mixed complex is obtained by taking Minkowski sums of shrunk Delaunay simplices and their dual Voronoi cells.

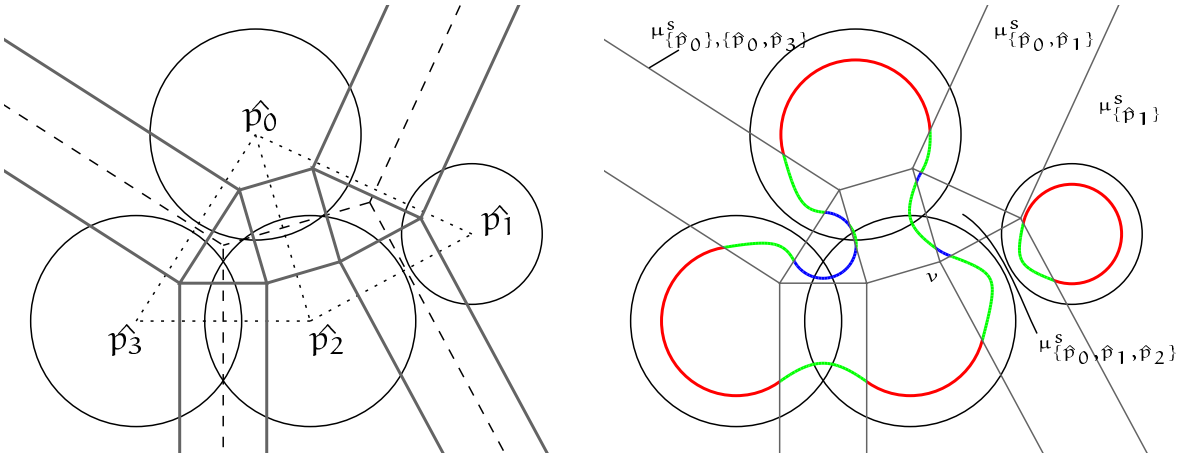

(a) The Delaunay triangulation (dashed), the Voronoi diagram (dotted) and the Mixed complex (solid).

(b) The mixed complex and some of the labels. Note that $\nu = \mu^s_{\{\hat{p}_0,\hat{p}_2\},\{\hat{p}_1,\hat{p}_2\}} = \mu^s_{\{\hat{p}_2\},\{\hat{p}_0,\hat{p}_1,\hat{p}_2\}}$.

Figure 5.2: The skin curve of four weighted points (the circles). Each mixed cell contains parts of an hyperbola or a circle.

Definition 42. *For* $\delta_{\mathcal{X}} \in \mathrm{Del}(\mathcal{P})$ *the* mixed cell $\mu^s_{\mathcal{X}}$ *is defined by* $\mu^s_{\mathcal{X}} = (1-s)\cdot \delta_{\mathcal{X}} \oplus s \cdot \nu_{\mathcal{X}}$.

Here $\cdot$ denotes the multiplication of a set by a scalar and $\oplus$ denotes the Minkowski sum. For $s = 0$ the mixed cell is the Delaunay cell. If s increases it deforms affinely into the Voronoi cell for $s = 1$.

Each mixed cell is a convex polyhedron since it is the Minkowski sum of two convex polyhedra. Based on the dimension of the Delaunay simplex, there are four types of mixed cells. A mixed cell of type ℓ corresponds to a Delaunay ℓ-cell and is of the form $\mu^s_{\mathcal{X}}$ with $|\mathcal{X}| = \ell + 1$. In 3D, mixed cells of type 3 are tetrahedra (shrunk Delaunay 3-cells) and mixed cells of type 0 are shrunk Voronoi 3-cells. A mixed cell of type 1 or 2 is a prism with respectively the shrunk Voronoi facet or the shrunk Delaunay facet as its base.

The intersection of the skin surface and a mixed cell is a piece of a sphere or a hyperboloid. In the plane, the intersection of a skin curve with a mixed cell is either part of a circle or hyperbola. An example of the mixed complex and a skin curve is given in Figure 5.2. All rectangles are mixed cells of type 1 and contain hyperbolic patches. The other cells contain circular arcs. Depending on whether the mixed cell is of type 0 or 2, the interior of the skin curve lies inside or outside the circle.

Within a mixed ℓ-cell $\mu^s_{\mathcal{X}}$, the skin surface is a quadratic surface of the form $I^{-1}_{\mathcal{X}}(0)$, where:

$$I_{\mathcal{X}}(x) = -\frac{1}{1-s}\sum_{i=1}^{\ell} x_i^2 + \frac{1}{s}\sum_{i=\ell+1}^{3} x_i^2 - R^2, \tag{5.1}$$

with $x = (x_1, x_2, x_3)$ and R^2 the weight of the weighted point in $\mathrm{aff}(\delta_{\mathcal{X}})$ centered at $f(\mathcal{X})$. More precisely, $\mathrm{skn}^s(\mathcal{X}) \cap \mu^s_{\mathcal{X}} = I^{-1}_{\mathcal{X}}(0) \cap \mu^s_{\mathcal{X}}$. The coordinate system is orthonormal with its origin at the focus of $\mathcal{X}$, and such that the first ℓ coordinates span the affine hull $\delta_{\mathcal{X}}$, see [48].

The following observation holds trivially for mixed cells of type 0 and 3. For mixed cells of type 1 and 2, the symmetry sets of the hyperboloids are the affine hulls of the corresponding Delaunay simplex and Voronoi cell. Hence it follows from the construction of the mixed cells.

Observation 43. *Each proper face of a mixed cell $\mu^s_{\mathcal{X}}$ is perpendicular to a symmetry set of $I_{\mathcal{X}}$*

Since the symmetry axis and the symmetry plane of the hyperboloid are perpendicular, each face of a mixed cell of type 1 or 2 is parallel to the other symmetry set.

Polyhedral complex The mixed complex is a polyhedral complex. The 3-cells of this polyhedral complex are formed by the mixed cells. We give a more detailed description of its structure.

Definition 44. *For $\mathcal{X}, \mathcal{X}' \subseteq \mathcal{P}$, with $\nu_{\mathcal{X}}, \nu_{\mathcal{X}'} \neq \emptyset$, a polyhedral cell $\mu^s_{\mathcal{X},\mathcal{X}'}$ is defined as $\mu^s_{\mathcal{X},\mathcal{X}'} = \mu^s_{\mathcal{X}} \cap \mu^s_{\mathcal{X}'}$.*

Edelsbrunner gives an intuitive picture of the mixed complex in [48]. Take the interval of d-dimensional affine subspaces of $\mathbb{R}^{d+1}$ defined by $x_{d+1} = s$, for $s \in [0, 1]$. Draw $\mathrm{Del}(P)$ in $x_{d+1} = 0$ and $\mathrm{Vor}(\mathcal{P})$ in $x_{d+1} = 1$. For each Delaunay simplex and corresponding Voronoi cell construct

$$\mu_{\mathcal{X}} = \mathrm{conv}(\delta_{\mathcal{X}} \cup \nu_{\mathcal{X}}).$$

All $\mu_{\mathcal{X}}$ are convex polyhedra of dimension $d+1$, their interiors mutually disjoint, and they decompose the strip between $x_{d+1} = 0$ and $x_{d+1} = 1$. The subspace $x_{d+1} = s$ intersects $\mu_{\mathcal{X}}$ in the mixed cell $\mu^s_{\mathcal{X}}$.

It is clear that a polyhedral cell $\mu^s_{\mathcal{X},\mathcal{X}'}$ is non-empty, for $0 < s < 1$, if the Delaunay and Voronoi cells of $\mathcal{X}$ and $\mathcal{X}'$ have a non-empty intersection. Or, equivalently, if $\nu_{\mathcal{X}\cap\mathcal{X}'}, \nu_{\mathcal{X}\cup\mathcal{X}'} \in \mathrm{Vor}(\mathcal{P})$. It is not enough for one of the two simplices to exists. E.g., let $\hat{p}_1, \hat{p}_2, \hat{p}_3$ be weighted points, the centers of which are the vertices of a triangle in a two-dimensional Delaunay triangulation and $\mathcal{X} = \{\hat{p}_1, \hat{p}_2\}$, $\mathcal{X}' = \{\hat{p}_3\}$. Then $\delta_{\mathcal{X}\cup\mathcal{X}'} \in \mathrm{Del}(\mathcal{P})$, but $\mathcal{X} \cap \mathcal{X}' = \emptyset$, hence $\delta_{\mathcal{X}\cap\mathcal{X}'} \notin \mathrm{Del}(\mathcal{P})$. On the other hand, let $\delta_{\mathcal{X}}$, $\delta_{\mathcal{X}'}$ be two Delaunay edges, that share a common vertex, but do not have an incident triangle in common, then $\delta_{\mathcal{X}\cap\mathcal{X}'} \in \mathrm{Del}(\mathcal{P})$, but $\delta_{\mathcal{X}\cup\mathcal{X}'} \notin \mathrm{Del}(\mathcal{P})$.

The following lemma describes the structure of the mixed complex.

Lemma 45. *A mixed cell $\mu^s_{\mathcal{X},\mathcal{X}'}$ is not empty iff $\nu_{\mathcal{X}\cap\mathcal{X}'}$ and $\nu_{\mathcal{X}\cup\mathcal{X}'}$ are nonempty In that case,*

$$\mu^s_{\mathcal{X},\mathcal{X}'} = (1 - s) \cdot \delta_{\mathcal{X}\cap\mathcal{X}'} \oplus s \cdot \nu_{\mathcal{X}\cup\mathcal{X}'}.$$

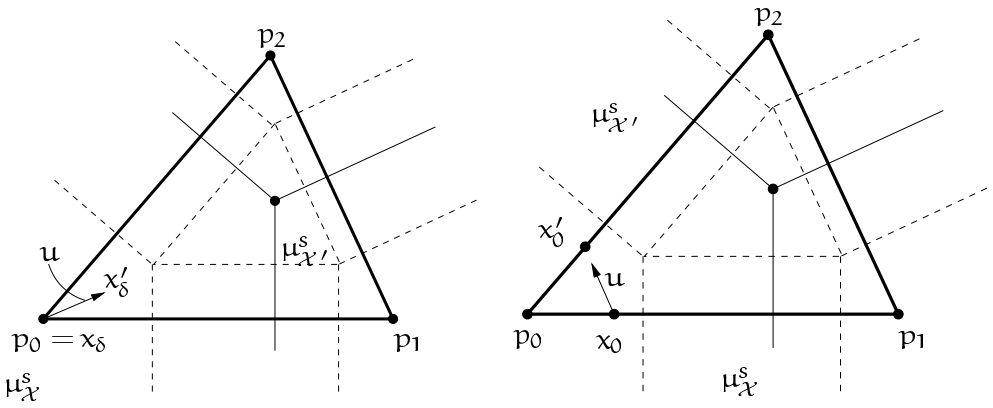

(a) $\mathcal{X} = \{\hat{p}_0\}, \mathcal{X}' = \{\hat{p}_0, \hat{p}_1, \hat{p}_2\}$, hence $\mathcal{X} \subseteq \mathcal{X}'$

(b) $\mathcal{X} = \{\hat{p}_0, \hat{p}_1\}, \mathcal{X}' = \{\hat{p}_0, \hat{p}_2\}$, hence $\mathcal{X} \not\subset \mathcal{X}'$ and $\mathcal{X}' \not\subset \mathcal{X}$

Figure 5.3: Illustration of the proof of Lemma 45.

Before we prove this lemma we first make some general remarks. Note that the lemma also holds if $\nu_{\mathcal{X}\cap\mathcal{X}'} = \emptyset$ or $\nu_{\mathcal{X}\cup\mathcal{X}'} = \emptyset$, since then $\mu^s_{\mathcal{X}} = \emptyset$.

Corollary 46. *If $\nu_{\mathcal{X}\cap\mathcal{X}'}$ and $\nu_{\mathcal{X}\cup\mathcal{X}'}$ are nonempty, then $\mu^s_{\mathcal{X},\mathcal{X}'} = \mu^s_{\mathcal{X}\cap\mathcal{X}',\mathcal{X}\cup\mathcal{X}'}$*

The corollary holds since, $\mu^s_{\mathcal{X}\cap\mathcal{X}',\mathcal{X}\cup\mathcal{X}'} = (1-s)\cdot\delta_{\mathcal{X}\cap\mathcal{X}'} \oplus s\cdot\nu_{\mathcal{X}\cup\mathcal{X}'}$. Hence, each non-empty polyhedral cell $\mu^s_{\mathcal{X},\mathcal{X}'}$ has a unique label, if $\mathcal{X} \subset \mathcal{X}'$. To gain some intuition for the lemma, take s equal to zero. Then the mixed complex is the Delaunay triangulation and indeed $\mu^0_{\mathcal{X},\mathcal{X}'} = \delta_{\mathcal{X}} \cap \delta_{\mathcal{X}'} = \delta_{\mathcal{X}\cap\mathcal{X}'}$. Conversely, for $s = 1$, the mixed complex is the Voronoi diagram and $\mu^1_{\mathcal{X},\mathcal{X}'} = \nu_{\mathcal{X}} \cap \nu_{\mathcal{X}'} = \nu_{\mathcal{X}\cup\mathcal{X}'}$.

Proof of Lemma 45. The proof is trivial if $\mathcal{X} = \mathcal{X}'$, hence we assume that $\mathcal{X} \neq \mathcal{X}'$. For simplicity, let $F = (1-s)\cdot\delta_{\mathcal{X}\cap\mathcal{X}'} \oplus s\cdot\nu_{\mathcal{X}\cup\mathcal{X}'}$.

From Definition (42) it follows that $F \subseteq \mu^s_{\mathcal{X}}$ and $F \subseteq \mu^s_{\mathcal{X}'}$, since $\delta_{\mathcal{X}\cap\mathcal{X}'} \subseteq \delta_{\mathcal{X}}, \delta_{\mathcal{X}'}$ and $\nu_{\mathcal{X}\cup\mathcal{X}'} \subseteq \nu_{\mathcal{X}}, \nu_{\mathcal{X}'}$. Hence, $F \subseteq \mu^s_{\mathcal{X},\mathcal{X}'}$.

For the opposite inclusion, we show that the two mixed cells lie in opposite halfspaces and intersect the bounding plane in F.

We distinguish two cases. First, consider the case where $\mathcal{X} \subseteq \mathcal{X}'$ or $\mathcal{X}' \subseteq \mathcal{X}$; See Figure 5.3(a). Without loss of generality we assume that $\mathcal{X} \subseteq \mathcal{X}'$. Let u be a vector perpendicular to $\delta_{\mathcal{X}}$ pointing from a point in $\delta_{\mathcal{X}}$ towards a point in the interior of $\delta_{\mathcal{X}'}$, such that $\langle u, x'_\delta - x_\delta\rangle > 0$, for $x_\delta \in \delta_{\mathcal{X}}$, $x'_\delta \in \delta_{\mathcal{X}'} \setminus \delta_{\mathcal{X}}$. Such a vector u exists, since $\delta_{\mathcal{X}}$ is a proper face of the convex polyhedron $\delta_{\mathcal{X}'}$. Note that u is perpendicular to $\delta_{\mathcal{X}}$. Lemma 41(2) states that $\langle u, x'_\nu - x_\nu\rangle < 0$, for $x_\nu \in \nu_{\mathcal{X}} \setminus \nu_{\mathcal{X}'}$, $x_\nu \in \nu_{\mathcal{X}'}$.

For each point x in a mixed cell $\mu^s_{\mathcal{X}}$ there exists a unique combination $x_\delta \in \delta_{\mathcal{X}}$, $x_\nu \in \nu_{\mathcal{X}}$, such that $x = (1-s)\cdot\delta_{\mathcal{X}} + s\cdot\nu_{\mathcal{X}}$, since $\delta_{\mathcal{X}}$ and $\nu_{\mathcal{X}}$ are affinely independent. Hence, since $F \subseteq \mu^s_{\mathcal{X}}$, a point $y_0 \in F$ can be uniquely written as $y_0 = (1-s)\cdot y^0_\delta + s\cdot y^0_\nu$ with $y^0_\delta \in \delta_{\mathcal{X}}$, $y^0_\nu \in \nu_{\mathcal{X}}$.

We analyze the sign of the inner product $\langle u, y - y_0\rangle$ for y subsequently in $\mu^s_{\mathcal{X}} \setminus F$, F and $\mu^s_{\mathcal{X}'} \setminus F$.

First, let $y \in \mu^s_{\mathcal{X}} \setminus F$. We write $y = (1-s)\cdot y_\delta + s \cdot y_\nu$, with $y_\delta \in \delta_{\mathcal{X}}$ and $y_\nu \in \nu_{\mathcal{X}} \setminus \nu_{\mathcal{X}'}$. The inner product $\langle u, y_\delta - y^0_\delta\rangle$ is zero since $y_\delta, y^0_\delta \in \delta_{\mathcal{X}}$ and $\langle u, y_\nu - y^0_\nu\rangle < 0$ by Lemma 41(2). Hence $\langle u, y - y_0\rangle < 0$ for $y \in \mu^s_{\mathcal{X}} \setminus F$.

Now assume that $y \in F$. Similar to y_0, we write $y = (1-s)\cdot y_\delta + s \cdot y_\nu$, with $y_\delta \in \delta_{\mathcal{X}}$, $y_\nu \in \nu_{\mathcal{X}'}$. The inner product $\langle u, y_\delta - y^0_\delta\rangle$ is zero since $y_\delta, y^0_\delta \in \delta_{\mathcal{X}}$ and $\langle u, y_\nu - y^0_\nu\rangle = 0$ by Lemma 41*(1)*.

Finally, assume that $y \in \mu^s_{\mathcal{X}'} \setminus F$, then we write y as $y = (1-s)\cdot y_\delta + s \cdot y_\nu$, with $y_\delta \in \delta_{\mathcal{X}'} \setminus \delta_{\mathcal{X}}$ and $y_\nu \in \nu_{\mathcal{X}'}$. The inner product $\langle u, y_\delta - y^0_\delta\rangle$ is positive by construction of u, and $\langle u, y_\nu - y^0_\nu\rangle = 0$, again by Lemma 41*(1)*. Hence $\langle u, y - y_0\rangle > 0$ for $y \in \mu^s_{\mathcal{X}'} \setminus F$.

Summarizing, we have:

$$\langle u, y - y_0\rangle \begin{cases} < 0, & \text{for } y \in \mu^s_{\mathcal{X}} \setminus F, \\ = 0, & \text{for } y \in F, \\ > 0, & \text{for } y \in \mu^s_{\mathcal{X}'} \setminus F. \end{cases}$$

Hence, $\mu^s_{\mathcal{X}}$ and $\mu^s_{\mathcal{X}'}$ lie in opposite halfspaces and meet only in F.

We continue with the proof of the second case. Assume that $\delta_{\mathcal{X}}$ is not a face of $\delta_{\mathcal{X}'}$ and vice versa. Then $\mathcal{X} \cap \mathcal{X}' \subsetneq \mathcal{X}, \mathcal{X}' \subsetneq \mathcal{X} \cup \mathcal{X}'$, viz. Figure 5.3(b). For this case the proof is similar, except for the construction of the vector u.

Let $x_I \in \delta_{\mathcal{X}\cap\mathcal{X}'}$. The Delaunay simplex $\delta_{\mathcal{X}\cap\mathcal{X}'}$ has at least co-dimension 2, since $|\mathcal{X} \cup \mathcal{X}'| - |\mathcal{X} \cap \mathcal{X}'| \geq 2$. Hence, the set of points orthogonal to $\delta_{\mathcal{X}\cap\mathcal{X}'}$ through x_I is at least 2-dimensional. We intersect this orthogonal set with a small sphere centered at x_I. If the radius is small enough, the intersection contains a point $x_0 \in \mathrm{int}(\delta_{\mathcal{X}})$ and $x'_0 \in \mathrm{int}(\delta_{\mathcal{X}'})$.

Let $u = \gamma \cdot (x'_0 - x_0)$, for some $0 < \gamma < 1$. By construction the triangle x_I, x_0, x'_0 is perpendicular to $\delta_{\mathcal{X}\cap\mathcal{X}'}$. Since $\|x_I - x_0\| = \|x_I - x'_0\|$, the triangle x_I, x_0, x'_0 is an isosceles triangle. Hence, the angles $\angle x_I, x_0, x'_0$, $\angle x_I, x'_0, x_0$ are equal and acute. As a result, for $y_0 \in \delta_{\mathcal{X}\cap\mathcal{X}'}$ we have:

$$\langle u, y - y_0\rangle \begin{cases} < 0, & \text{for } y \in \delta_{\mathcal{X}} \setminus \delta_{\mathcal{X}\cap\mathcal{X}'}, \\ = 0, & \text{for } y \in \delta_{\mathcal{X}\cap\mathcal{X}'}, \\ > 0, & \text{for } y \in \delta_{\mathcal{X}'} \setminus \delta_{\mathcal{X}\cap\mathcal{X}'}. \end{cases}$$

Note that u points from x_0 towards the interior of $\delta_{\mathcal{X}\cup\mathcal{X}'}$. Hence, u satisfies Lemma 41 with respect to $\delta_{\mathcal{X}}$ and $\delta_{\mathcal{X}\cup\mathcal{X}'}$. Using a similar argument, $-u$ satisfies Lemma 41 with respect to $\delta_{\mathcal{X}'}$ and $\delta_{\mathcal{X}\cup\mathcal{X}'}$. So, for $y_0 \in \nu_{\mathcal{X}\cup\mathcal{X}'}$ we have:

$$\langle u, y - y_0\rangle \begin{cases} < 0, & \text{for } y \in \nu_{\mathcal{X}} \setminus \nu_{\mathcal{X}\cup\mathcal{X}'}, \\ = 0, & \text{for } y \in \nu_{\mathcal{X}\cup\mathcal{X}'}, \\ > 0, & \text{for } y \in \nu_{\mathcal{X}'} \setminus \nu_{\mathcal{X}\cup\mathcal{X}'}. \end{cases}$$

Now we combine the results for the Delaunay simplices and the Voronoi cells to a statement for the mixed cell. Let $y_0 \in F$ and write y_0 as $y_0 = (1-s)\cdot y^0_\delta + s \cdot y^0_\nu$ with $y^0_\delta \in \delta_{\mathcal{X}}$, $y^0_\nu \in \nu_{\mathcal{X}'}$.

Write $y \in \mu^s_{\mathcal{X}} \setminus F$ uniquely as $y = (1-s)\cdot y_\delta + s \cdot y_\nu$, with $y_\delta \in \delta_{\mathcal{X}}$ and $y_\nu \in \nu_{\mathcal{X}}$. Since $y \notin F$, either $y_\delta \notin \delta_{\mathcal{X}\cap\mathcal{X}'}$ or $y_\nu \notin \nu_{\mathcal{X}\cup\mathcal{X}'}$. Expand the inner product

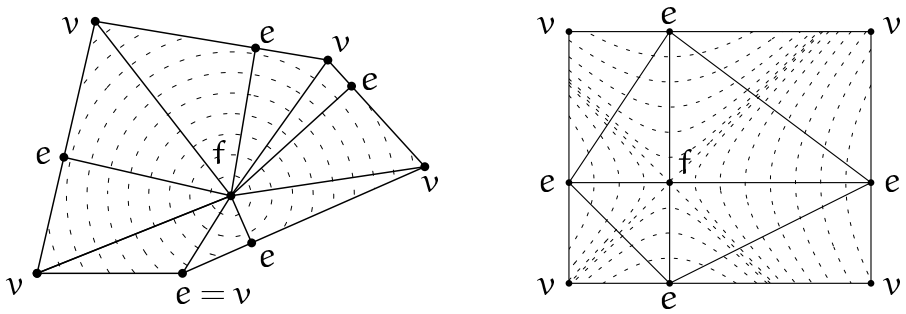

(a) Circular facets (b) Hyperbolic facets

Figure 5.4: The anchor points of two-dimensional polyhedral cells. Each anchor point is labeled by the type its cell (f for face, e for edge and v for vertex). The triangulation constructed in Section 5.3.2 is also shown.

$\langle u, y - y_0 \rangle$ to $(1-s) \cdot \langle u, y_\delta - y^0_\delta \rangle + s \cdot \langle u, y_\nu - y^0_\nu \rangle$. Using the estimates above, we obtain $\langle u, y - y_0 \rangle < 0$

A similar reasoning yields $\langle u, y - y_0 \rangle = 0$ for $y \in F$ and $\langle u, y - y_0 \rangle > 0$ for $y \in \mu^s_{\mathcal{X}} \setminus F$. □

Denote with $\mathrm{aff}(X)$ the affine hull of a set X.

Lemma 47. *For $\mathcal{X} \subset \mathcal{X}'$, $\mathrm{aff}(\mu^s_{\mathcal{X},\mathcal{X}'})$ and $\mathrm{aff}(\delta_{\mathcal{X}'}) \cap \mathrm{aff}(\nu_{\mathcal{X}})$ are complementary and orthogonal.*

Proof. To shorten notation we write $F = \mathrm{aff}(\mu^s_{\mathcal{X},\mathcal{X}'})$ and $G = \mathrm{aff}(\delta_{\mathcal{X}'}) \cap \mathrm{aff}(\nu_{\mathcal{X}})$. Recall from Lemma 45 that $\mu^s_{\mathcal{X},\mathcal{X}'} = (1-s) \cdot \delta_{\mathcal{X}} \oplus s \cdot \nu_{\mathcal{X}'}$.

The cells $\delta_{\mathcal{X}}$ and $\nu_{\mathcal{X}'}$ are affinely independent, hence $\dim F = \dim \delta_{\mathcal{X}} + \dim \nu_{\mathcal{X}'} = d + |\mathcal{X}| - |\mathcal{X}'|$. Further, $\delta_{\mathcal{X}'}$ and $\nu_{\mathcal{X}}$ are orthogonal and $\dim G = \dim \mathrm{aff}(\delta_{\mathcal{X}'}) - \dim \mathrm{aff}(\delta_{\mathcal{X}}) = |\mathcal{X}'| - |\mathcal{X}|$. Hence, the dimensions of F and G add up to d. Both $\delta_{\mathcal{X}}$ and $\nu_{\mathcal{X}'}$ are orthogonal to G, which shows the orthogonality of F and G. □

Corollary 48. *The dimension of a non-empty mixed cell $\mu^s_{\mathcal{X},\mathcal{X}'}$ in $\mathbb{R}^d$, is $d - |\mathcal{X} \cup \mathcal{X}'| + |\mathcal{X} \cap \mathcal{X}'|$.*

5.2.4 The anchor point

For the construction of the mesh we use the anchor point of a polyhedron.

Definition 49. *Let A be a convex set and p a point in $\mathbb{R}^3$. Then the* anchor point $a_p(A)$ *is the point in A closest to p.*

We are interested in the case where A is a polyhedral cell $\mu^s_{\mathcal{X},\mathcal{X}'}$, a Delaunay cell $\delta_{\mathcal{X}}$ or a Voronoi cell $\nu_{\mathcal{X}}$ and p is the focus $f(\mathcal{X})$. In fact, we use the anchor points of the polyhedral cells as vertices of a tetrahedral complex that decomposes the skin surface into topological disks.

We distinguish two types of critical points on a mixed cell $\mu^s_{\mathcal{X}}$, interior critical points are critical points of $I_{\mathcal{X}}$ contained in the interior of $\mu^s_{\mathcal{X}}$ and boundary critical points are critical points of $I_{\mathcal{X}}$ restricted to the boundary of $\mu^s_{\mathcal{X}}$. All critical points are anchor points of a face of the mixed cell, viz. Figure 5.4. However, not all anchor points are critical points, e.g. the point that is both the anchor point of a vertex and an edge in Figure 5.4(a).

Lemma 50. *A (boundary or regular) critical point of* $I_{\mathcal{X}}$ *on a polyhedral cell* $\mu^s_{\mathcal{X},\mathcal{X}'}$ *is the anchor point of* $\mu^s_{\mathcal{X},\mathcal{X}'}$ *or the anchor point of one of its faces with respect to* $f(\mathcal{X})$.

Proof. The focus $f(\mathcal{X})$ is the only critical point of the quadratic function $I_{\mathcal{X}}$. If $f(\mathcal{X})$ is contained in $\mu^s_{\mathcal{X},\mathcal{X}'}$, then it is the anchor point $a_{f(\mathcal{X})}(\mu^s_{\mathcal{X},\mathcal{X}'})$.

It remains to show that all boundary critical points are also anchor points. By Observation 43, a face of $\mu^s_{\mathcal{X},\mathcal{X}'}$ is either parallel or perpendicular to the symmetry sets of $I_{\mathcal{X}}$. Hence, if $f(\mathcal{X})$ projects onto the facet, then the facet has a boundary critical point. By definition, this point is the anchor point of the facet with respect to $f(\mathcal{X})$. □

Let $\mu^s_{\mathcal{X},\mathcal{X}'}$ be a common face of $\mu^s_{\mathcal{X}'}$ and $\mu^s_{\mathcal{X}}$. The following lemma shows that the anchor points of $\mu^s_{\mathcal{X},\mathcal{X}'}$ with respect to $f(\mathcal{X})$ and $f(\mathcal{X}')$ are identical.

Lemma 51. $a_{f(\mathcal{X})}(\mu^s_{\mathcal{X},\mathcal{X}'}) = a_{f(\mathcal{X}')}(\mu^s_{\mathcal{X},\mathcal{X}'})$.

Proof. Both $f(\mathcal{X})$ and $f(\mathcal{X}')$ lie on $\operatorname{aff}(\delta_{\mathcal{X}\cup\mathcal{X}'})$ and $\operatorname{aff}(\nu_{\mathcal{X}\cap\mathcal{X}'})$ by definition. Hence they lie on $\operatorname{aff}(\delta_{\mathcal{X}\cup\mathcal{X}'})\cap\operatorname{aff}(\nu_{\mathcal{X}\cap\mathcal{X}'})$, which is orthogonal to $\mu^s_{\mathcal{X},\mathcal{X}'}$ by Lemma 47. □

The following lemma gives a relation between the anchor point of a polyhedral cell and the anchor points of Delaunay simplices and Voronoi cells.

Lemma 52. $a_{f(\mathcal{X})}(\mu^s_{\mathcal{X},\mathcal{X}'}) = (1-s)\cdot a_{f(\mathcal{X}\cap\mathcal{X}')}(\delta_{\mathcal{X}\cap\mathcal{X}'}) + s\cdot a_{f(\mathcal{X}\cup\mathcal{X}')}(\nu_{\mathcal{X}\cup\mathcal{X}'})$.

Proof. If A and B are orthogonal, then

$$a_{f(\mathcal{X})}(s\,A \oplus (1-s)\,B) = a_{f(\mathcal{X})}(s\,A) + a_{f(\mathcal{X})}((1-s)\,B).$$

Therefore, since $\delta_{\mathcal{X}\cap\mathcal{X}'}$ and $\nu_{\mathcal{X}\cup\mathcal{X}'}$ are orthogonal, we have $a_{f(\mathcal{X})}(\mu^s_{\mathcal{X},\mathcal{X}'}) = (1-s)\cdot a_{f(\mathcal{X})}(\delta_{\mathcal{X}\cap\mathcal{X}'}) + s\cdot a_{f(\mathcal{X})}(\nu_{\mathcal{X}\cup\mathcal{X}'})$.

Since $f(\mathcal{X}), f(\mathcal{X}\cap\mathcal{X}') \in \operatorname{aff}(\nu_{\mathcal{X}\cap\mathcal{X}'})$ and $\delta_{\mathcal{X}\cap\mathcal{X}'}$ is orthogonal to $\nu_{\mathcal{X}\cap\mathcal{X}'}$, we have $a_{f(\mathcal{X})}(\delta_{\mathcal{X}\cap\mathcal{X}'}) = a_{f(\mathcal{X}\cap\mathcal{X}')}(\delta_{\mathcal{X}\cap\mathcal{X}'})$. Similarly, $f(\mathcal{X}), f(\mathcal{X}\cup\mathcal{X}') \in \operatorname{aff}(\delta_{\mathcal{X}\cup\mathcal{X}'})$ and $\delta_{\mathcal{X}\cup\mathcal{X}'}$ is orthogonal to $\nu_{\mathcal{X}\cup\mathcal{X}'}$, hence $a_{f(\mathcal{X})}(\nu_{\mathcal{X}\cup\mathcal{X}'}) = a_{f(\mathcal{X}\cup\mathcal{X}')}(\nu_{\mathcal{X}\cup\mathcal{X}'})$. Concluding, $a_{f(\mathcal{X})}(\mu^s_{\mathcal{X},\mathcal{X}'}) = (1-s)\cdot a_{f(\mathcal{X}\cap\mathcal{X}')}(\delta_{\mathcal{X}\cap\mathcal{X}'}) + s\cdot a_{f(\mathcal{X}\cup\mathcal{X}')}(\nu_{\mathcal{X}\cup\mathcal{X}'})$. □

Now that we have the decomposition of the anchor point of a polyhedral cell into the anchor point of Delaunay and Voronoi cells, we show that these anchor points are easily constructed.

Lemma 53. *The anchor point* $a_{f(\mathcal{X})}(\delta_{\mathcal{X}})$ *lies in the interior of* $\delta_{\mathcal{X}}$ *or* $a_{f(\mathcal{X})}(\delta_{\mathcal{X}}) = a_{f(\mathcal{X}')}(\delta_{\mathcal{X}'})$, *where* $\delta_{\mathcal{X}'}$ *is a face of* $\delta_{\mathcal{X}}$

Proof. Assume that $f(\mathcal{X})$ is not contained in $\text{int}(\delta_{\mathcal{X}})$, otherwise the proof is trivial. Since $\delta_{\mathcal{X}}$ is a convex polyhedron, the point closest to $f(\mathcal{X})$ lies on a proper face of $\delta_{\mathcal{X}}$, say $\delta_{\mathcal{X}'}$.

Since $f(\mathcal{X}), f(\mathcal{X}') \in \text{aff}(\nu_{\mathcal{X}'})$ and $\delta_{\mathcal{X}'}$ is orthogonal to $\nu_{\mathcal{X}'}$, we have $a_{f(\mathcal{X})}(\delta_{\mathcal{X}'}) = a_{f(\mathcal{X}')}(\delta_{\mathcal{X}'})$. □

A similar lemma holds for Voronoi cells, for which we omit the proof.

Lemma 54. *The anchor point* $a_{f(\mathcal{X})}(\nu_{\mathcal{X}})$ *lies in the interior of* $\nu_{\mathcal{X}}$ *or* $a_{f(\mathcal{X})}(\nu_{\mathcal{X}}) = a_{f(\mathcal{X}')}(\nu_{\mathcal{X}'})$*, where* $\nu_{\mathcal{X}'}$ *is a face of* $\nu_{\mathcal{X}}$

Concluding, from the anchor points $a_{f(\mathcal{X})}(\delta_{\mathcal{X}})$ and $a_{f(\mathcal{X})}(\nu_{\mathcal{X}})$, with $\delta_{\mathcal{X}} \in \text{Del}(\mathcal{P})$ we can construct the anchor point of any polyhedral cell. Moreover, Lemma 53 and Lemma 54 give a recursive definition that makes it easy to compute $a_{f(\mathcal{X})}(\delta_{\mathcal{X}})$ and $a_{f(\mathcal{X})}(\nu_{\mathcal{X}})$.

5.3 The meshing algorithm

This section describes the construction of a tetrahedral complex for which the intersection of a cell with the skin surface is either empty or a topological disk. Moreover we show that the mesh extracted from this tetrahedral complex by the marching tetrahedra algorithm [92] is isotopic to the skin surface.

5.3.1 Monotonicity condition

In Section 5.3.2 we give a detailed construction of the tetrahedral complex. For now, we only give the main condition imposed on the tetrahedral complex. First, we require that each tetrahedron is contained in a single mixed cell. Recall that the skin surface restricted to a mixed cell $\mu^s_{\mathcal{X}}$ is a subset of the quadric $I_{\mathcal{X}}^{-1}(0)$, cf. Equation (5.1). Express a point $x = (x_1, x_2, x_3)$ in the local coordinate system of $I_{\mathcal{X}}$.

Condition 55 (Monotonicity). *Let* ab *be a line segment contained in a mixed cell* $\mu^s_{\mathcal{X}}$ *of type* ℓ*, with* $I_{\mathcal{X}}(a) \leq I_{\mathcal{X}}(b)$*. The segment* ab *satisfies the monotonicity condition if* $x_1^2 + \ldots + x_\ell^2$ *is non-increasing and* $x_{\ell+1}^2 + \ldots + x_3^2$ *is non-decreasing on the segment from* a *to* b*.*

In words, a segment ab satisfies the monotonicity condition if the distance to both symmetry sets of the quadric $I_{\mathcal{X}}$ is monotone and the distance to one symmetry set of $I_{\mathcal{X}}$ does not increase if the distance to the other symmetry set increases. For spheres ($\ell = 0, 3$) one symmetry set is empty and the monotonicity condition is satisfied if the distance to the center of the sphere is monotone. For hyperboloids ($\ell = 1, 2$) a segment satisfies the monotonicity condition if the distances to the symmetry axis and the symmetry plane are monotone and the distance to one symmetry set does not increase if the distance to the other symmetry set increases. From Equation (5.1) we conclude:

Observation 56. *If a line segment* $\mathtt{ab}$ *satisfies the monotonicity condition, then* $I_{\mathcal{X}}$ *is monotonically increasing on* $\mathtt{ab}$.

We construct the tetrahedral complex in such a way that all edges satisfy the monotonicity condition. In fact, if all edges satisfy the monotonicity condition, then a generalized monotonicity condition holds for all cells.

Lemma 57. *Let* $\mu^s_{\mathcal{X}}$ *be a mixed cell of type* ℓ *and let* $v_1, \ldots, v_n$ *be the vertices of a cell of the tetrahedral complex in* $\mu^s_{\mathcal{X}}$, *with* $I_{\mathcal{X}}(v_i) \leq I_{\mathcal{X}}(v_j)$ *if* $i < j$.

If the monotonicity condition holds for all edges then, each segment $\mathtt{ab}$, *with* $\mathtt{a} \in \mathrm{conv}(v_1, \ldots, v_k)$ *and* $\mathtt{b} \in \mathrm{conv}(v_{k+1}, \ldots, v_n)$, *for* $k \in \{1, \ldots, n\}$, *satisfies the monotonicity condition.*

In the proof we need a small lemma.

Lemma 58. *Let* $v_1v_2v_3$ *be a triangle in* $\mathbb{R}^2$, *such that the distance to the origin is monotonically increasing (decreasing) along both* v_1v_3 *and* v_2v_3. *Then the distance to the origin is monotonically increasing (decreasing) on the segment* xv_3, *with* $x \in v_1v_2$.

Proof. Let $x = (1-t)v_1 + tv_2$, with $t \in (0,1)$ and let $d(\gamma) = \| (1-\gamma)x + \gamma v_3 \|^2$ be the squared distance to the origin on the line segment xv_3. The distance $d(\gamma)$ is monotone if $d'(\gamma) \geq 0$ or $d'(\gamma) \leq 0$ for $\gamma \in [0,1]$. Since $d'(\gamma) = 2\langle x, v_3 - x\rangle + 2\gamma\langle v_3 - x, v_3 - x\rangle$, $d(\gamma)$ is monotone if $\langle x, v_3 - x\rangle \geq 0$ or $\langle v_3, v_3 - x\rangle \leq 0$.

Assume that the distance to the origin increases monotonically on both line segments v_1v_3 and v_2v_3, hence $\langle v_1, v_3 - v_1\rangle \geq 0$ and $\langle v_2, v_3 - v_2\rangle \geq 0$. We have

$$\begin{aligned} \langle x, v_3 - x\rangle &= (1-t)\langle v_1, v_3 - v_1\rangle \\ &\quad + t\langle v_2, v_3 - v_2\rangle \\ &\quad + t(1-t)\| v_2 - v_1 \|^2 \\ &\geq 0. \end{aligned}$$

Conversely assume that the distance to the origin decreases monotonically on both line segments v_1v_3 and v_2v_3, hence $\langle v_3, v_3 - v_1\rangle \leq 0$ and $\langle v_3, v_3 - v_2\rangle \leq 0$. Then we have $\langle v_3, v_3 - x\rangle = (1-t)\langle v_3, v_3 - v_1\rangle + t\langle v_3, v_3 - v_2\rangle \leq 0$. □

Proof of Lemma 57. We repeatedly move vertices along edges of the cell of the tetrahedral complex while maintaining the monotonicity condition. After the displacement of the vertices, the line segment $\mathtt{ab}$ lies on one of the edges.

Since $I_{\mathcal{X}}(v_i) \leq I_{\mathcal{X}}(v_j)$ for $i < j$ and by Equation (5.1), the distance to the symmetry set spanned by the first ℓ coordinate axis is decreasing and the distance to the other symmetry set is increasing. Assume for now that if we move the vertices v_i and v_{i+1} over the edge v_iv_{i+1}, that all edges in the new cell satisfy the monotonicity condition.

We now move v_1 to $\mathtt{a}$ and v_n to $\mathtt{b}$. If $k = 1$, then $\mathtt{a}$ is v_1. Otherwise we move v_{k-1} to v_k until $\mathtt{a}$ lies on the face $\mathrm{conv}(v_1, \ldots, v_{k-1})$ and repeat this step for $k-1$. Similarly we move v_{k+1} to v_{k+2} until $\mathtt{b}$ lies on the face $\mathrm{conv}(v_{k+1}, \ldots, v_n)$ and

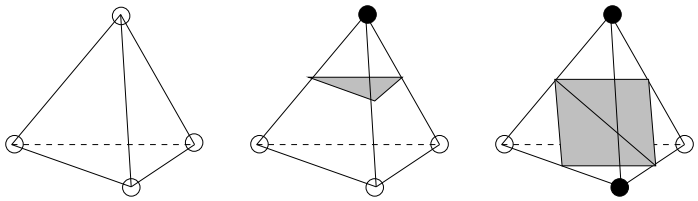

Figure 5.5: The three different configurations of a tetrahedron. White and black vertices lie on different sides of the skin surface.

repeat the step for $k+1$ until $k = n-1$. Then ab is an edge of the new tetrahedron. Hence ab satisfies the monotonicity condition.

It remains to show that the new edges also satisfy the monotonicity condition. Therefore consider three vertices v_i, v_{i+1} and v_j. If $j < i$ ($j > i+1$) then the distance to the first symmetry set along the line segment v_jv_i and v_jv_{i+1} is decreasing (increasing) and to the second symmetry set it is increasing (decreasing). We show that the distances remain monotonically increasing or decreasing along a line segment xv_j for $x \in v_iv_{i+1}$. We distinguish three cases. First, assume that the symmetry set is a point. We project the symmetry point on the plane $v_jv_iv_{i+1}$. From the previous lemma it follows that the distance on xv_j to the projection of the symmetry point is monotone, and therefore also the distance to the symmetry point. Next, assume that the symmetry set is a line, then we project the triangle $v_jv_iv_{i+1}$ on a plane orthogonal to the symmetry line. By applying the previous lemma, it follows that the distance to the projection of the line on the plane along the line segment xv_j is monotone. Finally, if the symmetry set is a plane we do not need the previous lemma. In this case the distance to the plane at x is smaller (greater) than the distance at v_j. Hence the distance to the symmetry plane on xv_j is monotone.

To conclude, if the distance to a symmetry set is monotonically increasing (decreasing) along both v_jv_i and v_jv_{i+1}, then this distance is also monotonically increasing (decreasing) along the line segment xv_j, with $x \in v_iv_{i+1}$. Hence xv_j satisfies the monotonicity condition. □

Mesh extraction The coarse mesh is extracted from the tetrahedral complex by the marching tetrahedra algorithm [92]. Each edge of the tetrahedral complex intersects the skin surface at most once by Observation 56. We place vertices of the mesh on these intersection points. Then the mesh is constructed by considering the number of vertices of the tetrahedron inside the skin surface as depicted in Figure 5.5. The third configuration remains ambiguous, since the common interior edge of the two triangles can be flipped.

Theorem 59. *A tetrahedral complex for which each edge satisfies the monotonicity condition has two properties:*

1. *each cell intersects the skin surface in a topological disk and*

2. *the mesh extracted from the tetrahedral complex is isotopic to the skin surface.*

Proof. Let V^- and V^+ be the vertices of a k-cell of the tetrahedral complex inside and outside the skin surface, respectively. Consider the set of line segments ab with $\mathsf{a} \in \text{conv}(V^-)$, $\mathsf{b} \in \text{conv}(V^+)$. The set of line segments is empty if the cell does not intersect the skin surface, i.e. if $V^- = \emptyset$ or $V^+ = \emptyset$. On the other hand, if the cell intersects the skin surface, then the set of line segments spans the cell and the line segments may intersect but only at their endpoints. On faces of the cell, the line segments are defined consistently because there the construction is based only on the labels of vertices of the face.

By Lemma 57, each segment satisfies the monotonicity condition. Hence $\mathrm{I}_\mathcal{X}$ is monotone on ab. Moreover, a lies inside and b outside the skin surface. Therefore ab intersects the skin surface in a single point. Since the segments span the tetrahedron, the skin surface within the cell is a topological disk.

By construction, each segment also intersects the coarse mesh transversally in exactly one point. We construct the isotopy by constructing an isotopy between the mesh and the skin surface within each tetrahedron and by showing that the isotopies defined by two tetrahedra are identical on a common face.

Neither the skin surface nor the mesh intersects a tetrahedron with only inside (outside) vertices, and we define the isotopy by the identity function. If the skin surface intersects a tetrahedron, then the segments span the tetrahedron and each point in the tetrahedron and on the skin surface lies on a unique segment. The same holds for a point in the tetrahedron and on the mesh. We construct the isotopy by linearly moving each point on the skin surface along the segment to the mesh. By construction of the segments, this deformation is an isotopy.

To show that these local isotopies can be combined to form an isotopy between the skin surface and the coarse mesh it remains to show that the transition between two local isotopies is continuous. This follows from the construction of the segments on a common face, which depends only on the label of its vertices. □

We call the segments in the proof above *transversal segments* because each segment intersects both the skin surface and the coarse mesh transversally in a single point.

5.3.2 The tetrahedral complex

Up to now we assumed that it is possible to construct a tetrahedral complex in such a way that all edges satisfy the monotonicity condition. In this section we construct this tetrahedral complex. We triangulate polyhedral cells in order of increasing dimension.

All vertices of the tetrahedral complex are anchor points of polyhedral cells. In case an anchor point lies on the boundary of its polyhedral cell, it coincides with another anchor point and the simplicial complex is degenerate. Therefore, during the construction of the tetrahedral complex we test whether the anchor point lies in the interior of the polyhedral cell, and collapse the vertex otherwise. For simplicity, in the remainder of this section we assume that the anchor point lies in the interior of the mixed cell.

Subdividing polyhedral cells of positive co-dimension On each vertex of the polyhedral complex we place a vertex of the tetrahedral complex. Note that these vertices are the anchor point of 0-cells of the polyhedral complex.

Next, consider an edge $\mu^s_{\mathcal{X},\mathcal{X}'}$ of the polyhedral complex. By Lemma 50, if $I_{\mathcal{X}}$ has a critical point on the interior of the edge, this critical point is the anchor point of the edge. Therefore we split the edge in the anchor point $a_{f(\mathcal{X})}(\mu^s_{\mathcal{X},\mathcal{X}'})$ and construct two edges from the anchor point to the vertices. By Observation 43 a polyhedral edge is parallel to one symmetry set and is split in the point closest to the projection of the other symmetry set, hence both edges satisfy the monotonicity condition.

We distinguish two types of facets: *circular* facets are facets for which the contour lines of $I_{\mathcal{X}}$ restricted to the facet are circles. The other facets are called *hyperbolic* because the contour lines are hyperbolas on the facet. Since the skin surface is tangent continuous, $I_{\mathcal{X}}|\mu^s_{\mathcal{X},\mathcal{X}'} = I_{\mathcal{X}'}|\mu^s_{\mathcal{X},\mathcal{X}'}$ and the facet inherits the same type from both mixed cells $\mu^s_{\mathcal{X}}$ and $\mu^s_{\mathcal{X}'}$. All facets of mixed cells of type 0 and 3 are spherical. The facets of a mixed cell of type 1 or 2 are spherical if they touch a mixed cell of type 0 or 3, and hyperbolic if they touch a mixed cell of type 1 or 2.

We triangulate circular and hyperbolic facets differently. Circular facets are triangulated by adding an edge from the anchor point of the facet to each anchor point on the boundary of the facet, i.e., either the anchor point of an edge or a vertex. See Figure 5.4(a). Since the anchor point of the facet is the point closest to the center of the sphere, the distance to the focus increases monotonically on each edge and each edge satisfies the monotonicity condition.

Hyperbolic facets are rectangles with edges parallel or perpendicular to the symmetry axis of the corresponding hyperboloid. The anchor point of an edge is the point closest to the focus, hence it is the point on the edge closest to the symmetry axis the edge is orthogonal to. Similarly, the anchor point of the facet is the point on the facet closest to the focus. Thus the edges from the anchor point of the facet to the anchor point of an edge are parallel to one axis and the distance to the other axis increases monotonically. Further, we add edges from the anchor point of an edge to the anchor point of an orthogonal edge. On these edges the distance to one symmetry axis increases whereas the distance to the other symmetry axis decreases. This triangulation is depicted in Figure 5.4(b).

Subdividing polyhedral cells of type 0 and 3 The mixed cells of this type contain a spherical patch of the skin surface. Similar to spherical facets, we have to triangulate polyhedral cells of type 0 and 3 in such a way that the distance to the focus is monotone on each edge. The anchor point of the mixed cell is the point in the mixed cell closest to the focus. Hence the distance to the focus on each line segment from the anchor point of the mixed cell to any other point in the mixed cell is monotone, and therefore satisfies the monotonicity condition. We have already constructed the triangulation of the boundary of the mixed cell and triangulate the entire cell by adding edges from the anchor point of the cell to each vertex on the boundary. The tetrahedra are formed by taking the join of a triangle on the the triangulated boundary of the mixed cell and the anchor point of the mixed cell.

Subdividing polyhedral cells of type 1 and 2 The triangulation of mixed cells of type 1 and 2 is slightly more subtle. The mixed cell contains a hyperboloid patch of the skin surface and the mixed cell is a prism with its base parallel to the symmetry plane of the hyperboloid. For an edge to satisfy the monotonicity condition, the distance to both the symmetry plane and the symmetry axis has to be monotone and the distance to one symmetry set may not increase, if the distance to the other symmetry set increases.

We already triangulated the facets of the mixed cell. The hyperbolic facets of the prism are the facets that are parallel to the symmetry axis. We split the prism in the plane V through the anchor point of the mixed cell parallel to the symmetry plane. This plane also contains the anchor points of the faces and edges of the mixed cells that are parallel to the symmetry axis. Hence each facet parallel to the symmetry axis is already split in V. The new facet is spherical and we triangulate it accordingly.

Consider one split mixed cell. The base of the prism furthest away from the symmetry plane contains the points furthest away from the symmetry plane. Hence its anchor point is the point with maximal distance to the symmetry plane and minimal distance to the symmetry axis. Therefore, all line segments in the split mixed cell with this anchor point as a vertex satisfy the monotonicity condition. The boundary of the prism is already triangulated and we triangulate the split mixed cell by adding edges from the anchor point of the base to all vertices on the boundary. The tetrahedra are the join of a triangle on the triangulated boundary and the anchor point of the base.

Union of balls For a shrink factor one, the skin surface of a set of balls is the union of these balls. In this case, the mixed complex is the Voronoi diagram. This means that only mixed cells of type 0 are three-dimensional cells. This greatly simplifies the set of tetrahedra.

It is also desirable to retain edges of the mesh on the intersection of two balls. The subdivision algorithm ensures this by definition. Chew's algorithm can also be extended to allow constrained edges, see [34].

5.3.3 Complexity analysis

In many real world applications the size of the Delaunay triangulation is linear in the number of input balls, see [36, 10]. However, the worst case complexity of the Delaunay triangulation is quadratic in the number of input balls, see [22]. We show that the size of the coarse mesh is linear in the size of the Delaunay triangulation and that this is worst case optimal.

Lemma 60. *The size of the coarse mesh is linear in the size of the Delaunay triangulation.*

Proof. Because of the duality relationship, the size of the Voronoi complex is equal to the size of the Delaunay triangulation. Each mixed 0-cell (corresponding to a Delaunay vertex, is a shrunk Voronoi 3-cell, and its size is therefore equal to the

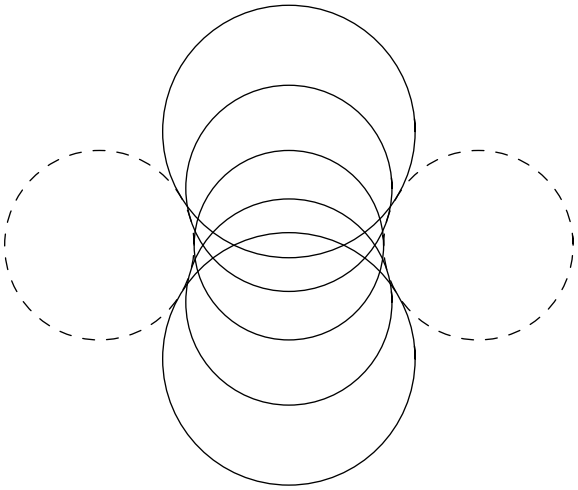

Figure 5.6: The cross section in the xz-plane of the skin surface with a quadatic number of holes. The centers of the dashed circles lie on the unit circle in the xy-plane and the centers of the solid circles on the z-axis.

Voronoi cell. Similarly, the complexity of a mixed 1-cell, 2-cell and 3-cell are linear in the complexity of the Voronoi facet, Delaunay facet and Delaunay tetrahedron.

We split each edge of the mixed complex at most in two parts. The triangulation of a mixed facet contains at most one triangle per split edge. Finally, the triangulation of a mixed cell contains at most one tetrahedron per triangle on the mixed facets. Hence, the size of the tetrahedral complex is linear in the mixed complex.

Within each tetrahedron we construct at most two triangles. Thus, the mesh is linear in the size of the Delaunay triangulation. □

To show that this is worst case optimal, we construct a skin surface with $\Omega(n^2)$ holes from a set of n balls. Any mesh with $\Omega(n^2)$ holes has complexity $\Omega(n^2)$, thus giving the lower bound. The construction, depicted in Figure 5.6, is as follows: the first $n/2$ balls are centered on the unit circle in the xy-plane and have radius 0.5. The other $n/2$ balls are centered on the z-axis. Their radius is such that they touch the first $n/2$ balls.

Each two subsequent spheres on the z-axis form a tunnel with each sphere centered on the unit circle. There are $n/2 - 1$ such pairs and $n/2$ spheres centered on the unit circle, hence there are $\Omega(n^2)$ tunnels. The skin surface also has $O(n^2)$ holes because it is homeomorphic to the union of the balls.

5.3.4 Mesh enhancement

The topologically correct mesh obtained with the marching tetrahedra algorithm is rather coarse and may contain long and skinny triangles. Therefore, we develop a method to enhance the mesh while maintaining the isotopy. The changes to the mesh we allow are local and do not change the topology of the mesh.

Before we change the mesh, we first test whether the isotopy with the skin surface is maintained. Therefore we use the transversal segments as described in the proof of Theorem 59. In fact, we first test whether each transversal line segment intersects the new mesh exactly once. We conclude this section with two examples of mesh refinement algorithms.

Changing the mesh To test whether the isotopy is maintained under a change of the mesh we would have to test whether each transversal line segment intersects the mesh once. We rephrase this in such a way that it is easier to verify.

Let c be a 3-cell in the tetrahedral complex, t a triangle of the mesh intersecting c and V^- and V^+ the vertices of c inside and outside the skin surface, respectively.

Lemma 61. *If for all* t *and* c, V^- *and* V^+ *are separated by the plane through* t *and* V^- *lies in the direction of the inner part of the mesh, then each transversal line segment within* c *intersects the mesh once.*

Proof. Consider a line segment $\mathsf{p}^-\mathsf{p}^+$, with $\mathsf{p}\pm \in \mathrm{conv}(V^\pm)$. Since p^- and p^+ lie on opposite sides of the mesh, $\mathsf{p}^-\mathsf{p}^+$ intersects the mesh at least once. Assume that it intersects $\mathsf{p}^-\mathsf{p}^+$ more than once, then on the second intersection point from p^-, the segment moves from outside the mesh to the inside. Hence. the inner product with the normal is negative. □

We now have an efficient way of testing whether the isotopy of the skin surface and the mesh is maintained. If the test fails, then the mesh is too coarse and we refine the mesh. We show that the refinement succeeds for small triangles.

Lemma 62. *A triangle* t *of the mesh contained in a single tetrahedron* c *can be subdivided in any point* $\mathsf{x} \in \mathsf{t}$ *by moving* x *along the transversal segments to the skin surface.*

Proof. Since x moves along the line segments within c, the line segments through f and the subdivided faces are the same. Thus the new mesh can be obtained from the old mesh by interpolation along the line segments. □

We can also flip an edge of the triangulation if the two adjacent triangles and the new triangles are intersected by the same transversal segments. This condition is similar to the condition in a two-dimensional mesh that an edge can be flipped if the union of the two triangles is convex.

To summarize, we have an efficient test to check whether the isotopy is maintained. If a change of the mesh would result in a violation of the isotopy test, then we can always subdivide the face into faces that are contained within a single tetrahedron. Each of these faces satisfies the isotopy test.

Sqrt-3 method We implemented the sqrt-3 subdivision method [69] on the coarse mesh. The sqrt-3 subdivision method splits each triangle into 9 sub-triangles and then moves the newly created vertices towards the skin surface along the transversal segments.

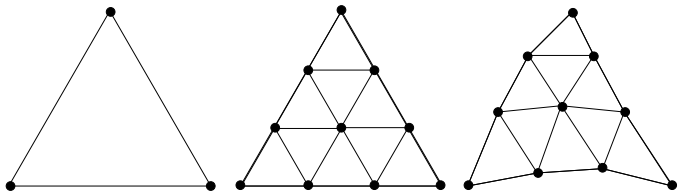

Figure 5.7: The Sqrt-3 subdivision method applied twice. Left: the original triangle, in the middle the subdivided triangle. On the right are the vertices placed on the skin surface.

By Lemma 62, the subdivision algorithm maintains the isotopy. Hence, it is not necessary to test isotopy, which make the algorithm very fast. On the other hand, the subdivision algorithm does not improve the quality of the triangles. Therefore this method is not suitable for constructing a mesh for numerical simulations.

Chew's algorithm We also implemented Chew's algorithm [34] to improve the quality of the triangles of the coarse mesh and obtain a mesh suitable for numerical simulations. After the algorithm terminates, each triangle has angles between 30 and 120 degrees and has a user defined maximal size. The only constraint on the size-criterion is that there exists a $\delta > 0$ such that any well-shaped triangle that fits within a circle of radius δ is well-sized. We chose the size of a triangles inversely proportional to the maximal curvature which is nonzero on skin surfaces.

During the refinement, we test the isotopy before an inserting a new point and before flipping an edge.

5.4 Implementation

We implemented the algorithm described above in C++ using the Computational Geometry Algorithm Library (CGAL) [37]. This algorithm will be available as a CGAL extension package.

CGAL is a library written in C++ that uses generic programming to attain its full flexibility. It can be subdivided in three parts: the kernel, datastructures and algorithms and supporting classes.

The kernel provides geometric primitive objects like points, line segments, triangles etc. The kernel also defines predicates and constructions on these objects. Predicates are functions that test a property (return a boolean). For example the "incirle test" used for the construction of the Delaunay triangulation is a predicate. Constructions are functions that return a geometric object, for example the intersection point of a line and a plane. Several kernels are provided in CGAL: (1) inexact predicates and inexact constructions, (2) exact predicates and inexact constructions and (3) exact predicates and exact constructions.

The second part of CGAL contains a collection of basic geometric data structures and algorithms, which are parameterized by traits classes that define the interface

between the data structure or algorithm and the primitives they use. Sometimes, the datastructures and algorithms are also parameterized by observer classes. Observer classes define functions that are called before or after an event occurs, they "observe" the algorithm.

The support library contains non-geometric support facilities, such as circulators, I/O support and interfaces between CGAL and various visualization tools, like geomview and QT.

5.4.1 Outline of the implementation

For the implementation of the algorithm the kernel is extended with a quadratic surface class to store the part of the skin surface contained inside a mixed cell.

We did not introduce new datastructures, but customized the datastructures available in CGAL to suit our needs. The weighted Delaunay triangulation is implemented in the `Regular_triangulation_3` class and does not need adaptations. The triangulated mixed complex `Triangulated_mixed_complex_3` is derived from the triangulation class `Triangulation_3` and has cells that additionally store a pointer to the quadratic surface defined inside the cells. The triangulated mesh is stored as a `Polyhedron_3`.

We implemented the function `triangulate_mixed_complex_3` that constructs the triangulated mixed complex from the Delaunay triangulation and the function `marching_tetrahedra_3` that extracts the triangulated mesh from the triangulated mixed complex. Further, we implemented the subdivision algorithm in the function `skin_surface_sqrt3` and a prototype of Chew's algorithm. An outline of the implementation is depicted in Figure 5.8.

No functionality was added to the support library.

In the remainder of this section we discuss the implementation in more detail. The kernels described below are the default kernels, everything can be customized using techniques like traits classes and templates.

Delaunay triangulation.

We use the `Regular_triangulation_3` to compute the weighted Delaunay triangulation of the input balls. Since no geometric objects are constructed during the construction of the Delaunay triangulation, any kernel with exact predicates produces the correct Delaunay triangulation.

Triangulated mixed complex.

The triangulated mixed complex is a `Triangulation_3`. Its kernel should also be able to do exact constructions, since the vertices of the triangulation are anchor points of simplices of the Delaunay triangulation, which are constructed. To speed up the computation, we use a filtering technique [24] that is present in CGAL. This filter first computes small boxes containing the vertices and uses those in further computations. If the filtered computations fail to give a guaranteed result, the computation is redone with an exact number type.

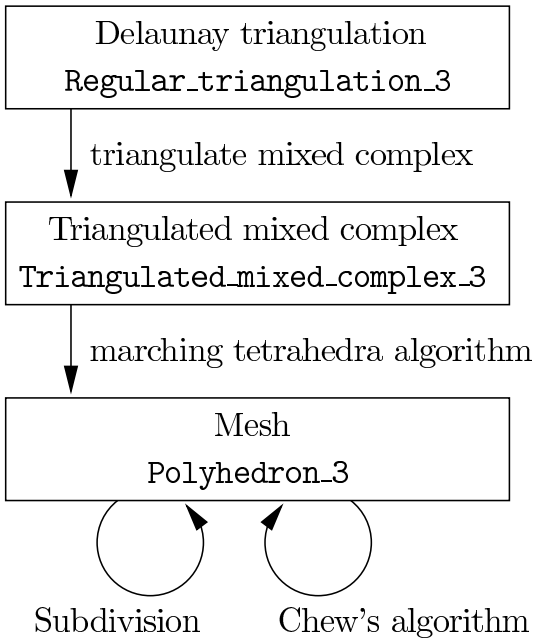

Figure 5.8: Outline of the implementation. The boxes contain the datastructures (with the name of the datastructure above the name of the class) and the labeled arrows denote the functions that construct one datastructure from the other. The labels describe the functions.

By definition, every tetrahedron in the triangulation is contained in a single mixed cell. We store a pointer to the quadratic surface corresponding to the mixed cell with each cell (tetrahedron). In this way we are able to move a point contained in the cell towards the skin surface. This is done by first constructing the transversal segment containing the point form the cell and then intersecting the transversal segment with the quadratic surface.

Mesh

For the mesh, we use the `Polyhedron_3` class which is able to store any orientable 2-manifold. The kernel has to be able to perform exact constructions since its vertices are constructed. Further the kernel has to support the predicates exactly that are needed in the refinement step.

Construction of the triangulated mixed complex

The construction of the triangulated mixed complex is the least straightforward part of the algorithm. It uses a `Triangulation_incremental_builder_3` that is developed for this algorithm, but might be of general interest. This builder first gets the vertices of the triangulation and then the cells, which are defined by references to four vertices. From these vertices and cells it constructs the triangulation.

The function `triangulate_mixed_complex_3` computes the vertices and cells of the triangulation and inserts them in the `Triangulation_incremental_builder_3`.

The construction of vertices is complicated due to the occurrence of many degenerate cases. For example, let $\nu_{\mathcal{X}}$ be a Voronoi edge and let $\nu_{\mathcal{X}'}, \nu_{\mathcal{X}''}$ be its two vertices. If the Voronoi edge degenerates into a point, then the anchor points $\mathfrak{a}_{\mathfrak{f}(\mathcal{X})}(\nu_{\mathcal{X}})$, $\mathfrak{a}_{\mathfrak{f}(\mathcal{X})}(\nu_{\mathcal{X}'})$ and $\mathfrak{a}_{\mathfrak{f}(\mathcal{X})}(\nu_{\mathcal{X}''})$ are equal. Similar cases occur if a Voronoi facet degenerates into a line segment or a Voronoi cell into a facet. We first compute the anchor points of the triangulated mixed complex and combine anchor points that are equal using a union-find datastructure. We then insert all unique vertices and the tetrahedra that are not degenerate, i.e., have four distinct vertices.

A similar class exists for the triangulation of the Voronoi diagram. This triangulation can be used for meshing the boundary of the union of a set of balls.

Marching tetrahedra algorithm

The marching tetrahedra algorithm `marching_tetrahedra_3` introduced in [92] takes four arguments: the triangulation, the polyhedron, a traits class and an observer class. The algorithm is performed on the triangulation and stored in the polyhedron. The `Polyhedron_incremental_builder_3` is used for constructing the polyhedron.

The traits class defines a single predicate and a construction. First it is able to test whether a vertex of the triangulation lies inside or outside the surface and it is able to return an intersection point of the surface with an edge of the triangulation whose vertices lie on opposite sides of the surface. For skin surfaces the intersection point is unique as is shown in Theorem 59.

The observer class implements two functions that are called after the construction of a vertex and a facet of the polyhedron. After insertion of a vertex in the polyhedron a function is called with the vertex of the polyhedron and the corresponding edge of the triangulation. Similarly, after insertion of a facet in the polyhedron a function is called with the facet of the polyhedron and the corresponding cell of the triangulation. Using these two functions it is possible to construct a reference from simplices of the mesh to the corresponding simplices of the triangulation.

Both the traits class and the observer class make this algorithm highly flexible.

Refinement algorithms

We also implemented both algorithms described in the Section 5.3.4. The implementation of the $\sqrt{3}$-subdivision method is straightforward. For the position of the new vertices, we use point location in the triangulated mixed complex and then project the new vertex along the transversal segment towards to the skin surface.

Initially, the performance of the subdivision algorithm was disappointing since the filtered point location step failed often leading to slow running times. This failure can be explained since new vertices of subdivided polyhedron lie on edges of the coarse mesh, which in turn lie in facets of the triangulation. Filtered arithmetic often fails in degenerate situations like this. To give the algorithm a significant speedup, we also store with each facet of the polyhedron a pointer to the cell of the triangulation entirely containing the facet. In this way the point location step

Molecule	Our algorithm			Dynamic	Marching
	Coarse	Sqrt-3	Chew		
pdb7tmn	0:00:01	0:00:02	0:00:05	0:10:00	0:00:05
DNA	0:00:14	0:00:29	0:00:55	0:35:12	0:00:51
Gramacidin A	0:00:08	0:00:31	0:01:13	1:35:23	0:03:22

Table 5.1: Performance comparison

is not necessary. Storing this pointer is done with an adapted observer class of the marching tetrahedra algorithm.

The implementation of Chew's algorithm is the only part that is still in a developmental stage. Before we apply Chew's algorithm we perform a preprocessing step in which we remove small edges. This reduces the size of the final mesh considerably.

5.5 Examples and experiments

We compare our algorithm to the algorithms described in [27] and [29]. There is a comparison of the two algorithms in [29]. These tests are run on a Pentium 4 running at 2.54GHZ. To test our algorithm we used an AMD Athlon 1800+ which is actually a little slower. We tested our algorithm on various molecules, computing only the coarse mesh, computing the coarse mesh and after that one $\sqrt{3}$-subdivision step and the coarse mesh which was subsequently improved using Chew's algorithm. For timings see Table 5.1.

Note that both our algorithm and the marching algorithm [29] are significantly faster than the dynamic skin algorithm [27]. However, [29] does not come with topological guarantees.

Figure 5.10 shows the molecule pdb7tmn. In Figure 5.10(d) we enlarged a part of the coarse mesh and applied the Sqrt-3 method in Figure 5.10(e). Note that the triangles remain skinny. Figure 5.10(f) shows the result of applying Chew's algorithm directly to the coarse mesh. Because of small edges in the coarse mesh, there are also small edges near parts with low curvature. If we remove small edges, as in Figure 5.10(g), before we apply Chew's algorithm, we obtain Figure 5.10(h).

5.6 Extension to envelope surfaces

We think that it is possible to adapt the algorithm presented in this chapter to mesh envelope surfaces, introduced in Chapter 4.

The main change lies in the construction of the triangulation of the generalized mixed complex defined in Section 4.4, Proposition 34. Similar to mixed complex of the skin surface, this polyhedral complex decomposes the envelope surface into pieces of quadrics. The function defined within a cell (of any dimension) of the polyhedral complex is a quadric. Any (non-degenerate) quadric has a unique critical point. We

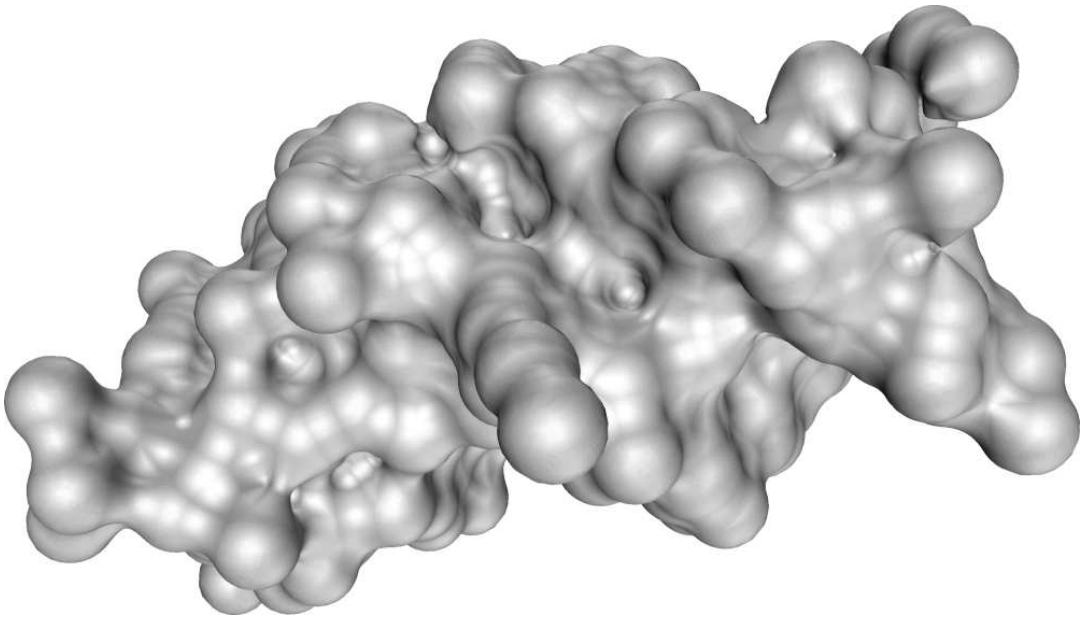

(a) DNA

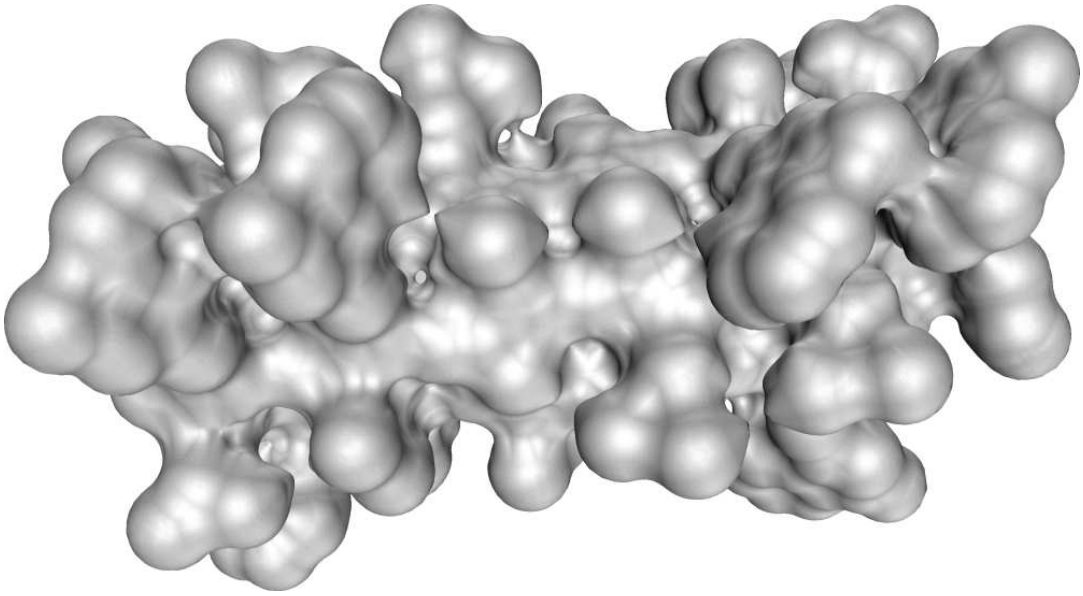

(b) Gramacidin A

Figure 5.9: Two larger molecules.

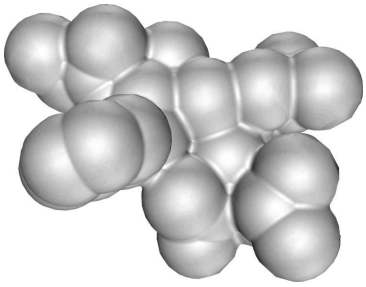

(a) Shrink: .85

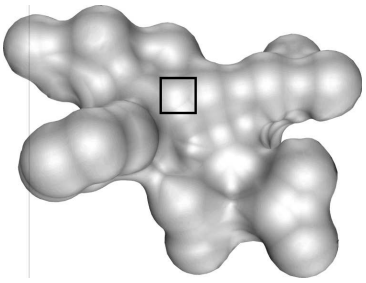

(b) Shrink: .5

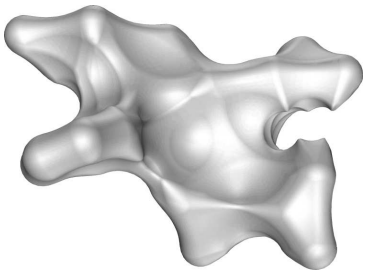

(c) Shrink: .15

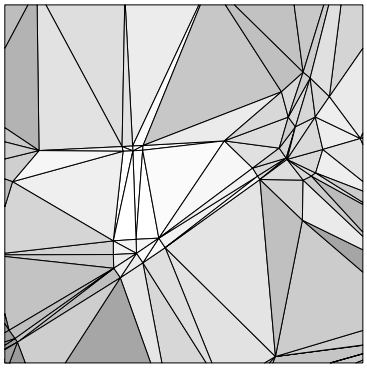

(d) Coarse mesh

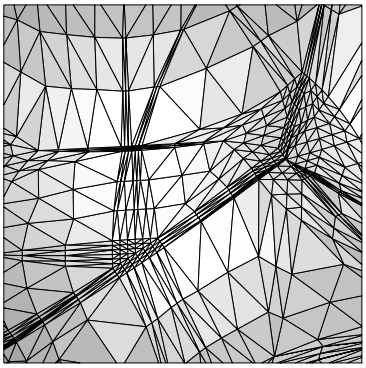

(e) Sqrt3-method

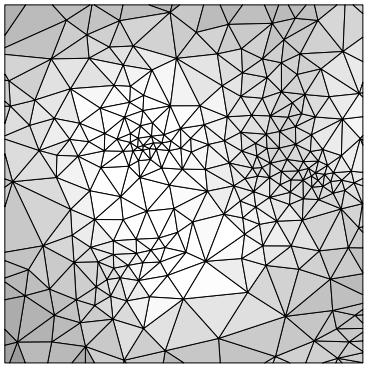

(f) Chew applied to the coarse mesh

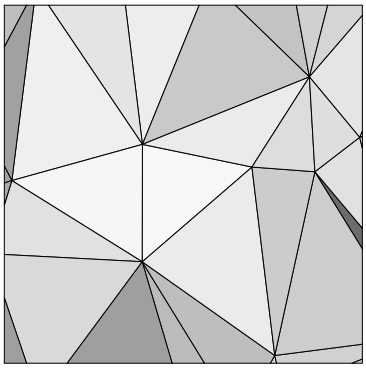

(g) Small edges removed

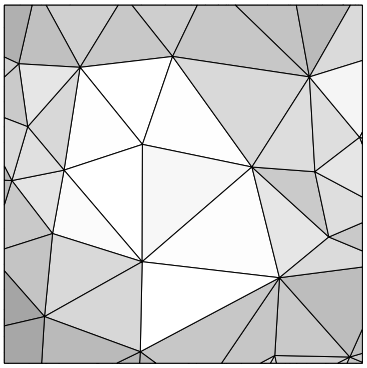

(h) Chew applied to the enhanced mesh

Figure 5.10: The molecule pdb7tmn.

define the vertices of the triangulated polyhedral complex as the anchor points of polyhedral cells with respect to the critical point of the quadric.

Next, we construct a triangulation such that all edges have the monotonicity condition. Therefore, we write the quadric in normal form using the eigenvectors as its basis and we split the polyhedral cell along the planes through the critical points spanned by two eigenvectors. For each non-empty clipped polyhedral cell, we first triangulate the facets of lower dimensional simplices and then construct interior edges. For the triangulation of facets we repeat the algorithm. The triangulation of the interior of the polyhedral cell is done such that on each edge the distance to a basisvector is non-decreasing (non-increasing) along the edge if the corresponding eigenvalue is positive (negative). This implies that all edges satisfy the monotonicity condition and that it is possible to construct the transversal segments. Using these segments we are able to prove Theorem 59 for the general case of envelope surfaces.

5.7 Conclusion and future work

We present an algorithm that constructs a mesh that is isotopic to the skin surface and discuss two methods to refine this mesh.

The algorithm we present is static in the sense that it generates a mesh for a fixed set of input balls.

Maintaining the coarse mesh while deforming the input set, is important for animations and deforming molecules. Two deformation schemes seem computationally interesting. From Lemma 52 we know that the anchor point of a mixed cell $\mu^{\mathrm{s}}_{\mathcal{X},\mathcal{X}'}$ only depends on the Delaunay cell $\delta_{\mathcal{X}\cup\mathcal{X}'}$, the Voronoi cell $\nu_{\mathcal{X}\cap\mathcal{X}'}$ and the shrink factor. Adding a constant to all weights does not change the Delaunay and Voronoi diagram and hence does not change the simplicial complex. Hence, the coarse mesh of the skin surface obtained by adding a constant to each weight is another level-set of the tetrahedral complex. Another deformation is obtained by varying the shrink factor. Again, the structure of the mixed complex and simplicial complex remains unchanged, however the positions of the anchor points change. It is sufficient to reposition the anchor points and then update or recompute the coarse mesh. In general, the solid foundation of the simplicial complex makes us believe that it is possible to maintain the simplicial complex if the Delaunay triangulation can be maintained.

We also believe that the algorithm can be generalized to mesh envelope surfaces that are presented in Chapter 4. For this purpose, we have to implement the changes proposed in Section 5.6. These changes do not seem to make the algorithm much more complicated and is interesting to implement the algorithm in the future and see how this algorithm performs for envelope surfaces.

Similar adaptations make the algorithm suitable for meshing Connelly surfaces. These surfaces are also used in molecular biology and are formed by a small probe sphere that carves away the space outside a union of balls. The disadvantage of this type of surfaces is that they may not be tangent continuous.